

# Brownian Dynamics of Flexible Polymers in Flow

R. Rzehak, A. Arend, D. Kienle, W. Zimmermann\*

## Abstract

The shape and the dynamics of flexible polymers in flow are described by bead–spring models taking into account hydrodynamic interactions and excluded volume effects. The Brownian dynamics of these models with many degrees of freedom and nonlinear interactions is simulated by algorithms that achieve a high efficiency. We consider a single tethered polymer in uniform flow as a simple model problem that has been studied recently both theoretically and experimentally. Here, we focus especially on hydrodynamic screening effects without employing commonly used averaging approximations. Potential applications to situations of biological interest are discussed.

## 1 Introduction

Flexible polymers are large chainlike molecules that consist of many parts with statistically independent orientation, the so-called Kuhn segments [1, 2]. They can assume a great variety of different arrangements in space which are termed conformations. The time scales for conformational changes of flexible polymers cover a very wide range. There are modes of the polymer dynamics with relaxation times which are as slow as the macroscopic hydrodynamic modes. Therefore, the microscopic and macroscopic degrees of freedom do not decouple in a simple manner as for simple fluids like water. The rich and at times surprising viscoelastic behavior of polymer solutions is a consequence of this coupling between individual polymer molecules and the flow field [1-4].

The interplay between the polymer molecules and a flow seems to be governed by two elementary processes: 1) How does a flow field deform a

---

\*R. Rzehak and D. Kienle: IFF Forschungszentrum Jülich, D-52425 Jülich; A. Arend and W. Zimmermann: Theoretische Physik, Universität des Saarlandes, D-66041 Saarbrücken;

polymer and 2) how does the motion of the polymer perturb the flow field? In the past, the quantitative analysis of the polymer–flow interaction causing the deformation of the polymer has been hampered by two difficulties. On the experimental side, the classic measurement techniques such as rheometry, birefringence, light scattering, and small angle neutron scattering provide only volume averaged quantities from which only little can be deduced about the behavior of the individual polymer molecules, let alone the flow field. On the theoretical side, the large number of polymer degrees of freedom which are coupled by various nonlinear interactions makes a treatment of the polymer–flow interaction on a fundamental level a formidable task.

Only recently a huge step forward in understanding the flow-induced polymer deformation has been achieved by studying single DNA molecules. DNA is much larger than synthetic polymers and can be manipulated with optical tweezers. When decorated by fluorescent dyes, the action of flows on the polymer can be followed under an optical microscope [6-9]. Thus DNA provides an ideal model system to study conformations of deformed polymers.

On the theoretical side, modern high-speed supercomputers allow to attack nonlinear problems with many degrees of freedom by means of numerical simulation. An advantage of computer simulation is that all observables are accessible in full detail which facilitates the investigation of features like the flow around the polymer which have not yet been resolved experimentally. Furthermore, this approach allows to compare different models in order to assess the importance of various interactions in different parameter regimes. This provides guidelines for developing more simplified models like effective dumbbell [4] or blob models [10-13] which neglect a large number of internal degrees of freedom of the polymer. Such models may then be used as building blocks for the description of more complicated systems (see *e.g.* [15]).

A variety of bead-spring polymer models which give a faithful representation of chain flexibility and are well suited for computer simulation is presented in sect. 2. These models include several important interactions: a finite extensibility of the springs, the excluded volume of the beads (**EVI**), and hydrodynamic interactions between the beads (**HI**). We put special emphasis on the latter which is responsible for the perturbation of the flow field. So far, bead–spring models have been investigated mostly with various averaging approximations for the HI [16, 17, 18]. In contrast to these works we keep the full conformation dependence of the HI by employing the so-called Oseen-approximation without any averaging.

A central issue in computer simulation is to devise efficient algorithms such that problems of interesting size and complexity can be tackled. At first sight, Brownian dynamics simulations with fluctuating HI require  $\mathcal{O}(N^3)$  operations, but with an approximation due to Fixman [19] the operation count

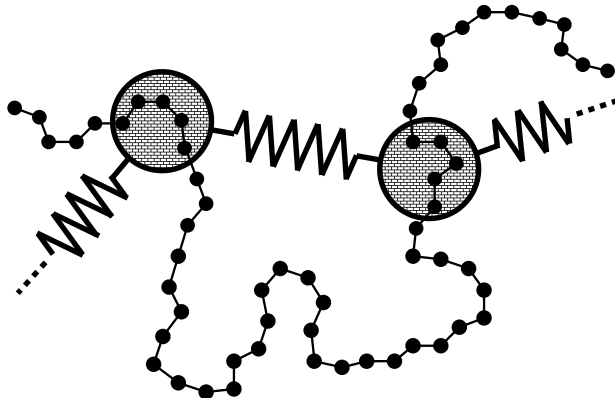


Figure 1: Sketch of the coarse-graining procedure leading to the bead-spring model. The small solid circles represent chemical groups in the backbone of the polymer with the solid lines indicating chemical bonds between them. The large shaded circles are the beads which are connected by springs reflecting the entropic elasticity of the subchain.

is reduced to  $\sim \mathcal{O}(N^{2.25})$  operations. For the EVI, book-keeping techniques familiar in molecular dynamics can be adapted to Brownian dynamics. These methods are described in sect. 3.

As an illustrative application we consider in sect. 4 a simple model problem, namely a single tethered polymer which is subjected to a uniform flow. This problem has been studied recently both experimentally [6, 7] and theoretically [10, 11, 20, 21]. Here, we discuss some advances that have been made using simulations [12, 13].

## 2 Bead-Spring Models for Polymer Dynamics

To study the long-time dynamics of polymers in dilute solution, coarse-grained models are used because atomistic models of long polymer chains are intractable even numerically with present-day computing equipment. A common class of such models are the so-called bead-spring models [22] where coarse-graining (cf. fig. 1) is achieved by replacing a subchain of a real polymer by a bead and a spring with a suitable force-elongation law [2, ?]. Friction and mass of the subchains are lumped into the beads as depicted in fig. 1. For a flexible chain each subchain corresponds to one or more Kuhn segments [2]. The solvent acts as a heat bath which causes a stochastic motion of the polymer.

Usually, one considers the motion on the diffusive timescale only, *i.e.* bead inertia are neglected [23]. The equation of motion for the position of the  $i$ -th bead ( $i = 1 \dots N$ ) is then obtained from a balance between all forces acting on the beads. These forces comprise viscous drag forces  $\mathbf{F}^H$  on one side and spring- and stochastic forces  $\mathbf{F}^\Phi$ ,  $\mathbf{F}^S$  on the other:

$$-\mathbf{F}_i^H = \mathbf{F}_i^\Phi + \mathbf{F}_i^S. \quad (1)$$

The drag forces are proportional to the difference between the velocity of a bead  $\mathbf{V}_i$  and the flow velocity at its position  $\mathbf{u}^0(\mathbf{R}_i)$ :

$$-\mathbf{F}_i^H = \zeta (\mathbf{V}_i - \mathbf{u}^0(\mathbf{R}_i)). \quad (2)$$

The single bead friction coefficient  $\zeta$  is given by Stokes law, *i.e.*  $\zeta = 6\pi\eta a$ , where  $\eta$  is the solvent viscosity and  $a$  is the effective hydrodynamic radius of a bead. In thermal equilibrium of course  $\mathbf{u}^0 \equiv \mathbf{0}$ . The stochastic forces are related to the dissipative drag by the fluctuation-dissipation theorem in order to ensure the correct equilibrium distribution. We have

$$\mathbf{F}_i^S = \sqrt{2k_B T \zeta} \xi_i, \quad (3)$$

where  $T$  is the solvent temperature,  $k_B$  is the Boltzmann constant and  $\xi_i$  is an uncorrelated Gaussian white noise with zero mean, *i.e.*

$$\begin{aligned} \langle \xi(t) \rangle &= \mathbf{0}, \\ \langle \xi(t) \xi^T(t') \rangle &= \delta(t - t') \mathbf{1}. \end{aligned} \quad (4)$$

Taking velocities and positions of *all* beads together as single supervectors for the velocity  $\mathbf{V}$  and position  $\mathbf{R}$ , the equations of motion may be written in the following general form:

$$\mathbf{V} \equiv \frac{\partial}{\partial t} \mathbf{R} = \mathbf{u}^0(\mathbf{R}) + \mathbf{H} \cdot (-\nabla_{\mathbf{R}} \Phi) + \sqrt{2k_B T \mathbf{H}} \xi. \quad (5)$$

Here we introduced a potential  $\Phi$  for the spring forces and the mobility  $\mathbf{H}$  which is the inverse of the friction coefficient,  $\zeta^{-1}$ . In the most general case to be discussed later on,  $\mathbf{H}$  will no longer be a simple scalar but a tensor which couples all beads. Boundary conditions are implemented by introducing additional beads with indices  $i = 0, N + 1$  which do not participate in the dynamics. Then for free chain ends we have  $\mathbf{R}_0 = \mathbf{R}_1$  viz.  $\mathbf{R}_{N+1} = \mathbf{R}_N$  while for fixed ends  $\mathbf{R}_0$  viz.  $\mathbf{R}_{N+1}$  are constant. Choosing  $k_B T = 1.0$  and  $\zeta = 1.0$  basically fixes units for energy and time. The remaining unit for length is the bondlength  $b$  to be discussed below.

The Rouse model [24] is the simplest conceivable polymer model which embodies only the chain connectivity by assuming harmonic springs, *i.e.* by using in eq. (5),

$$\Phi \equiv \Phi_{\text{H}} = \sum_i \frac{1}{2} k_{\text{H}} |\mathbf{R}_{i+1} - \mathbf{R}_i|^2. \quad (6)$$

For the force constant  $k_{\text{H}}$  we use a value of 3.0 such that the root mean square bond length in equilibrium  $b$  becomes unity. The mobility in the Rouse model is simply a scalar, namely the inverse of the single bead friction coefficient, *i.e.*  $\mathbf{H} = \zeta^{-1} \mathbf{1}$ . All of the above assumptions are tacitly introduced in order to make the equation of motion eq. (5) linear so that it may be solved analytically.

There are three obvious refinements each of which renders the equation of motion eq. (5) nonlinear: a finite extensibility of the springs, the excluded volume of the beads (EVI), which may be chosen such that the chain cannot cross itself, and hydrodynamic interactions between the beads (HI).

Since chemical bonds have a fixed length, real polymers are inextensible. This can be modeled by a nonlinear spring law which keeps the stretching of the springs small even for large forces. Rather common in simulations is the phenomenological FENE (**F**initely **E**xtensible **N**onlinear **E**lastic) spring law [25] with the potential

$$\Phi \equiv \Phi_{\text{F}} = - \sum_i \frac{1}{2} k_{\text{F}} R_{\text{F}}^2 \ln \left( 1 - \frac{|\mathbf{R}_{i+1} - \mathbf{R}_i|^2}{R_{\text{F}}^2} \right). \quad (7)$$

Another approach is to make the chain completely unstretchable by replacing the springs with rigid rods. In numerical simulations this may be achieved to a good approximation by augmenting the FENE spring law by a nearest-neighbor repulsion of the form described in eq. (8) below [26]. The values  $k_{\text{F}} = 30.0$  for the force constant and  $R_{\text{F}} = 1.5$  for the maximum extension of the spring then result in a bond length of  $b = 0.961$ . Obviously the effects of finite extensibility are most important when the polymer is driven far from equilibrium where the chain may be strongly stretched.

The excluded volume effect arises because different beads cannot occupy the same region in space. This is modeled by a repulsive interaction between any pair of beads as described *e.g.* by a truncated Lennard-Jones potential [26]

$$\Phi_{\text{LJ}} = \begin{cases} \sum_{i,j} 4\epsilon \left( \left( \frac{\sigma}{|\mathbf{R}_j - \mathbf{R}_i|} \right)^{12} - \left( \frac{\sigma}{|\mathbf{R}_j - \mathbf{R}_i|} \right)^6 + \frac{1}{4} \right) & \text{for } |\mathbf{R}_j - \mathbf{R}_i| < R_{\text{LJ}} \\ 0 & \text{for } |\mathbf{R}_j - \mathbf{R}_i| \geq R_{\text{LJ}}. \end{cases} \quad (8)$$

Here  $\epsilon$  and  $\sigma$  define energy and length scales of the excluded volume interaction and  $R_{\text{LJ}} = 2^{1/6}\sigma$  is the minimum of the conventional 6-12 Lennard-Jones potential. This term is included in the potential  $\Phi$  in eq. (5) along with the spring potential. When combined with harmonic springs the choice  $\epsilon = \sigma = 1.0$  gives an effective equilibrium bond length of  $b = 1.33$  as discussed in appendix A. Together with the FENE potential for the springs the bead-spring chain becomes self-avoiding like a real polymer for the parameters chosen [26]. The effects of excluded volume are most prominent in or close to thermal equilibrium where the polymer chain assumes a coil shape. Far from equilibrium, where the polymer chain is strongly stretched and the beads are far apart from each other, the excluded volume force tends to zero.

The hydrodynamic interaction (HI) is an effective interaction between any pair of beads which is mediated by the solvent. It arises in the following way: If the solvent exerts a drag force on a bead then by virtue of Newton's third law there must be a drag reaction force of the same strength but with reverse direction acting as a driving force for the solvent. According to eq. (1) the average of this force is given by the potential force  $-\nabla_{\mathbf{R}} \Phi$ . Neglecting the finite bead diameter – *i.e.* idealizing the drag reaction force as a point force – and using the linear equations of Stokes flow for the solvent dynamics, one can derive a general expression for the perturbation  $\mathbf{u}'$  of the imposed flow field resulting from the drag reaction forces of all beads [2, 27]:

$$\mathbf{u}'(\mathbf{R}_i) = \sum_{j \neq i} \Omega(\mathbf{R}_i - \mathbf{R}_j) \cdot (-\nabla_{\mathbf{R}_j} \Phi). \quad (9)$$

The  $i$ -th bead is excluded from the sum on the *rhs* of eq. (9) in order to suppress unphysical hydrodynamic self-interactions. The Stokes friction force on bead  $i$  as given by eq. (2) now arises from the bead velocity relative to the *perturbed* flow field  $\mathbf{u}^0 + \mathbf{u}'$ . Using this perturbed flow field instead of  $\mathbf{u}^0$  alone in eq. (5) and collecting all terms containing  $-\nabla_{\mathbf{R}} \Phi$ , one identifies the components of the mobility, which has now become a conformation dependent supermatrix, as

$$\mathbf{H}_{ij} = \begin{cases} \frac{1}{\zeta} \mathbf{1} & \text{for } i = j \\ \Omega(\mathbf{R}_i - \mathbf{R}_j) & \text{for } i \neq j \end{cases}. \quad (10)$$

Here the Oseen tensor [2] is nothing but the Greens function for Stokes flow,

$$\Omega(\mathbf{r}) = \frac{1}{8\pi\eta|\mathbf{r}|} (\mathbf{1} + \hat{\mathbf{r}}\hat{\mathbf{r}}^T). \quad (11)$$

It suffers from the deficiency that it becomes non-positive at small bead separations. Therefore it is necessary to introduce EVI along with HI [12]

or to use a regularization of the Oseen tensor [28]. So far we considered deterministic forces only. In order to complete the equation of motion for the case with HI, we need to specify the stochastic forces. Fortunately, it turns out that the fluctuation–dissipation theorem for this case has precisely the same form as before [29].

The choice  $\eta = 0.2$  for the solvent viscosity, with the bead radius  $a$  determined from  $6\pi\eta a = \zeta = 1.0$ , results in a value of  $h^* = \sqrt{\frac{3}{\pi}} \frac{a}{b} \approx 0.25$  for the dimensionless parameter  $h^*$  measuring the strength of the HI. This value is compatible with other work [30].

The collective effect of the hydrodynamic interactions is often condensed in the so-called non–draining assumption, *i.e.* the assumption that the polymer coil may be replaced by a sphere with some effective radius into which the external flow does not penetrate. This assumption is inspired by Zimm’s calculation of the diffusion coefficient of a polymer coil with HI [31] which is given by an expression similar to that of a hard sphere [2]. Apart from additional approximations in the calculation (see below) this evidence seems rather scarce support for the conclusion drawn. Only recently the perturbed flow field has been calculated directly [13] and this calculation revealed that the flow is weakened inside the polymer coil but not completely suppressed as shown in fig. 2. Furthermore, there is a significant penetration depth where the flow remains strong and a large long range effect that are neglected in the simple traditional picture.

If any of the three effects discussed above is to be included in the model without further approximations, one has to rely on numerical simulation in order to solve the equation of motion. Only if we restrict ourselves to the Rouse model with HI, an approximate treatment becomes possible by replacing  $\mathbf{H}(\mathbf{R})$  with its equilibrium average. This so-called preaveraging approximation has the effect of linearizing the equation of motion again. This procedure was proposed by Zimm [31] wherefore it is referred to as the Zimm model. Far from equilibrium the simple preaveraging approximation obviously breaks down. Various other approximation schemes have been proposed which avoid the use of the equilibrium distribution but which still lead to linear equations [16, 17, 18].

### 3 Efficient Brownian Dynamics Algorithms

The Brownian dynamics method pioneered by Ermack and McCammon [32] is nothing but the numerical integration of the Langevin equation eq. (5) with one realization of the stochastic process modeling the thermal noise. It yields one sample of polymer conformations  $\mathbf{R}(t_n)$  from which all quantities

of interest can be obtained as averages. Since several textbooks on the finite difference approximation of stochastic differential equations like eq. (5) are available [30, 33], we just briefly summarize our scheme and then move on to describe the efficient calculation of the various forces.

An important but not widely appreciated point in Brownian dynamics simulation concerns the accurate numerical reproduction of the equilibrium distribution [34]. Therefore, the usual procedure of trading accuracy for speed by choosing the time step so large that the algorithm is just stable is questionable here, because this might violate a fundamental physical principle. In order to cure this unfavorable situation Hendriks *et al* [34] suggested to introduce an artificial inertial term, *i.e.* to add  $m\ddot{\mathbf{R}}$  on the *lhs* of eq. (5). A stochastic velocity–Verlet scheme is then used to advance the solution in time. The final form of the numerical integration scheme with time step  $\delta t$  is

$$\begin{aligned} \mathbf{R}(t_n + \delta t) &= \mathbf{R}(t_n) + \mathbf{V}(t_n)\delta t + \frac{\delta t^2}{2m}\mathbf{F}(t_n), \\ m\mathbf{V}(t_n + \delta t) &= m\mathbf{V}(t_n) + \frac{\delta t}{2}(\mathbf{F}(t_n + \delta t) + \mathbf{F}(t_n)) \\ \mathbf{F}(t_n) &= \zeta \left( \sqrt{2k_{\text{B}}T\mathbf{H}(\mathbf{R}(t_n))} \Xi(t_n) \frac{1}{\sqrt{\delta t}} \right. \\ &\quad \left. - \left( \mathbf{H}(\mathbf{R}(t_n)) \frac{\partial\Phi}{\partial\mathbf{R}(t_n)} + \mathbf{V}(t_n) - \mathbf{u}^0(\mathbf{R}(t_n)) \right) \right). \end{aligned} \quad (12)$$

The random numbers  $\Xi$  are drawn from a uniform distribution on the interval  $[-\sqrt{3\delta t}, +\sqrt{3\delta t}]$  at each time  $t_n$ . This replacement of gaussian random numbers approximating the noise in eq. (5) is justified if only moments of the stochastic process  $\mathbf{R}(t_n)$  and not individual sample paths are sought [30].

As long as the mass is chosen small enough so the period of oscillations due to the added degrees of freedom is smaller than the diffusive time scale of the phenomena of interest, the results remain unaffected by the artificial inertia. As shown by the results in appendix A this condition is met for a value of  $m = 1.0$ . The time step  $\delta t$  then can be chosen up to a factor of 10 larger than in conventional BD (where the mass vanishes) if we require an error of less than 1% in the second moment of the equilibrium distribution for the positional degrees of freedom which can be calculated from the potentials given in sect. 2 (cf. appendix A). A value of  $\delta t = 0.02$  has been found suitable for all models.

The numerical algorithm eq. (12) was coded in standard FORTRAN90. A machine optimized version of the LAPACK library was used for the linear algebra calculations involved in the treatment of HI (see below). The simulations were performed on a single processor of a Cray T90 vector computer.

For the 200-bead chain with harmonic springs and both EVI and HI taken into account (cf. sect. 4), which is the most time-consuming case we considered, a maximal speed of 900 – 1000 MFLOPS was achieved. For shorter chains, of course, the vectorization is less efficient. Longer chains could not be treated for this model because the total requirement of CPU time – which was already  $\mathcal{O}(100h)$  for the flow field calculations in sect. 4 – becomes prohibitively large.

Several tests of the numerical scheme with respect to the equilibrium distribution of the bond length for the linear and nonlinear springs and the scaling of the root-mean-square end-to-end distance as a function of the number of beads are described in appendix A. The agreement with analytical solutions for these equilibrium properties is nearly perfect.

### 3.1 Evaluation of Stochastic Forces in the Presence of Hydrodynamic Interactions

A key issue for the present study with emphasis on HI is the calculation of the matrix  $\sqrt{\mathbf{H}}$  in eq. (5) and eq. (12) which is a function of all bead positions. To make the whole algorithm practical, an efficient way to evaluate the square root of the mobility matrix  $\mathbf{H}$  must be developed. The straight forward calculation of such an expression [35] involves a diagonalization of  $\mathbf{H}$  which numerically requires an effort of  $\mathcal{O}(N^3)$  machine instructions. A second standard method for the calculation of matrix functions is via series expansion of the desired function [35]. A Taylor series will contain only powers of the matrix argument which are easily evaluated numerically. However, matrix multiplication also requires  $\mathcal{O}(N^3)$  operations. A third method which again needs  $\mathcal{O}(N^3)$  operations but which offers the most favorable prefactor becomes possible by noting that the square root is not precisely what is needed. Instead one can also use the Cholesky decomposition of  $\mathbf{H}$ . This idea was exploited in the classic work by Ermak & McCammon [32]. In all cases the numerical effort of  $\mathcal{O}(N^3)$  makes the computation prohibitive for long chains. Therefore to our knowledge all previous Brownian dynamics studies of polymer dynamics which took HI into account were limited to chains with  $N \leq 20$  beads with one exception, the work of Fixman [36], where a few results for a chain of 56 beads are given.

An approximate method which requires only  $\sim \mathcal{O}(N^{2.25})$  operations was proposed later by Fixman [19]. The starting point for this method is an expression of the square root in terms of a complete set of polynomials as in

method two above, *i.e.*

$$\sqrt{\mathbf{H}} = \sum_{\mu=1}^M \mathcal{P}^{\mu}(\mathbf{H}). \quad (13)$$

A reduction of the computational effort becomes possible by noting that the knowledge of the matrix  $\sqrt{\mathbf{H}}$  is actually much more than what is really needed since once it is known it could be applied to *many different* random vectors  $\xi$ . For the simulation however it needs to be applied to *one single* realization only. A scheme which takes advantage of this is obtained by multiplying both sides of eq. (13) with  $\xi$ . Taking  $\xi$  into the sum on the *rhs* one obtains a series expression for  $\sqrt{\mathbf{H}} \xi$

$$\sqrt{\mathbf{H}} \xi = \sum_{\mu=1}^M \mathcal{P}^{\mu}(\mathbf{H}) \xi. \quad (14)$$

This expression contains only matrix–vector products and thus its evaluation requires an effort of  $\mathcal{O}(N^2)$  only. Furthermore the individual terms in the sum may be calculated recursively keeping the number of these operations low, too.

The polynomials  $\mathcal{P}^{\mu}(x)$  may be taken from *any* complete set in function space. The most economic choice are not simple powers  $\mathcal{P}^{\mu}(x) = x^{\mu}$  but Chebychev polynomials  $C^{\mu}(x)$  [37, 38]. These can be evaluated by means of the recursion relation

$$C^{\mu+1}(x) = 2x C^{\mu}(x) - C^{\mu-1}(x), \quad (15)$$

$$\text{with } C^1(x) = x,$$

$$\text{and } C^0(x) = 1. \quad (16)$$

Since the Chebychev polynomials are defined on the interval  $[-1, 1]$ , which is not suitable in the present context, one applies a transformation of the independent variable

$$x = \frac{2y}{b-a} - \frac{b+a}{b-a}, \quad (17)$$

which maps the domain of the problem  $y \in [a, b]$  to the domain  $x \in [-1, 1]$  of the Chebychev polynomials. The  $C^{\mu}(y)$  appear frequently in numerical analysis and are referred to as shifted Chebychev polynomials [37, 38].

If, as in the problem under consideration, the argument  $x$  is a matrix, not a simple scalar, then  $[a, b]$  is the range of eigenvalues of  $x$ . An estimate of

the range of the eigenvalues of  $\mathbf{H}$  is furnished by a simple physical argument: If two nearby beads experience a force in the same direction, the induced perturbations of the velocity field will have a large degree of coherence and thus add up to a larger perturbation. If on the other hand the forces are in opposite directions, the induced perturbations will cancel out to a large extent. Since beads which are neighbors along the chain are likely to be also close in space, an estimate for the largest eigenvalue is obtained by using a force vector with equal forces for all beads as a testvector  $\mathbf{F}$  to form the Rayleigh quotient [35]  $\mathbf{F}^T \mathbf{H} \mathbf{F} / \mathbf{F}^T \mathbf{F}$ . Similarly an estimate for the smallest eigenvalue is obtained by using a force vector with alternating forces for all beads as a testvector. In order to compensate for deviations of these estimates from the true values of largest and smallest eigenvalue of  $\mathbf{H}$  one takes a somewhat larger interval for the shifted Chebychev polynomials.

The order of truncation of the series,  $M$ , has to be determined empirically and increases somewhat with  $N$  whence the final effort grows with a somewhat higher power than 2. To monitor the accuracy of the approximation we compute the exact square root of  $\mathbf{H}$  via the spectral theorem using a QR algorithm [35] for the diagonalization whenever the conformation is saved. This happens only every 100 - 10000 time steps of the integration and is thus acceptable in terms of computer time.

### 3.2 Calculation of Excluded Volume Interactions

The most obvious way to calculate the excluded volume force on bead  $i$  is to loop over all other beads  $j$  checking whether they are within the interaction range  $R_{LJ}$  and if so calculating the force  $-\nabla\Phi_{LJ}$ . This leads to an algorithm where the total computational effort for calculating all EVI increases with the square of the number of beads. The short-range (in real space) nature of the forces leads to possible improvements since most pairs of beads  $i, j$  do not interact. Book-keeping methods that exploit this fact by keeping track of particles within the range of interaction are well known from the molecular dynamics literature [39, 40, 41]. One approach is to maintain for each bead  $i$  a so-called neighbor list giving the indices of beads  $j$  within a distance that is somewhat larger than the interaction range, *i.e.*  $|\mathbf{R}_i - \mathbf{R}_j| \leq R_{LJ} + R_s$ . In the actual force calculation then only the beads in this list have to be considered. As soon as the first bead has traversed the extra shell of thickness  $R_s$ , the list must be reconstructed from scratch. This step, which takes a time of order  $\mathcal{O}(N^2)$ , ultimately dominates the force computation such that an improvement of only a constant factor independent of  $N$  can be achieved. A second possibility is the cell list method where the space occupied by the beads is partitioned into cubic cells with edge length  $R_{LJ}$ . Having established

which beads fall in each cell, the calculation of the force on bead  $i$  needs to consider only beads  $j$  in the same and adjacent cells. This method has the desirable property that the effort is only of order  $\mathcal{O}(N)$ . To achieve full vectorization, it is necessary to use a layered datastructure [42]. A comparison [43] showed that in the context of molecular dynamics a combination of both approaches, where a neighbor list is built from a cell list, gives the fastest method.

Some preliminary experimentation indicated that this may be different in the case of nonequilibrium Brownian dynamics simulation. For a single stretched polymer the density of beads is extremely inhomogeneous. When the chain is placed in a quadrilateral box to set up a cell list, many cells will not contain any bead at all. Therefore, we use a simple neighbor list with a shell thickness of  $R_s = 0.5R_{LJ}$ , the value of which has been determined empirically. To implement a criterion when the list must be updated, we accumulate the displacement  $\delta\mathbf{R}$  each bead has undergone since the last update. The first bead has traversed the shell when  $\max_i(|\delta\mathbf{R}_i|) \geq R_s$ . Then an update of the neighbor list is necessary, which turns out to be the case approximately every 6th time step for the tests described in appendix A. On a workstation larger values of  $R_s \geq 10R_{LJ}$  turn out to be more advantageous leading to a list update only every 10th time step.

For  $N \gtrsim 1000$  the dominating part is the list update. The effort then continues to grow as  $\sim \mathcal{O}(N^2)$  (actually the power is somewhat less than 2 on the Cray because of gains due to better vectorization for longer chains). Compared to the force calculation without neighbor list this gives a speed-up of a constant factor of about 10 in an equilibrium situation. For a stretched polymer a somewhat larger gain is possible.

## 4 Results for a Simple Model Problem

In this subsection we describe results obtained in simulations of a bead-spring chain which is fixed at the origin with one end and subjected to a uniform flow in the  $x$ -direction. The chain has  $N = 200$  beads connected by harmonic springs and both EVI and HI are taken into account. For an unperturbed flow velocity  $\mathbf{u}^0 = (v, 0, 0)$  with  $v = 0.02$  we show in fig. 2a) the temporally averaged segment density  $\rho$  as a measure of the chain localization. The full flow field  $\mathbf{u}$  including the perturbation due to the HI between the beads is shown in fig. 2b). The flow velocity assumes its smallest values near the  $x$ -axis in the interval  $0 < x < 40$  where the beads are located with the largest probability. The important result emerging from these simulations is that the flow at the average location of the polymer coil does not vanish.

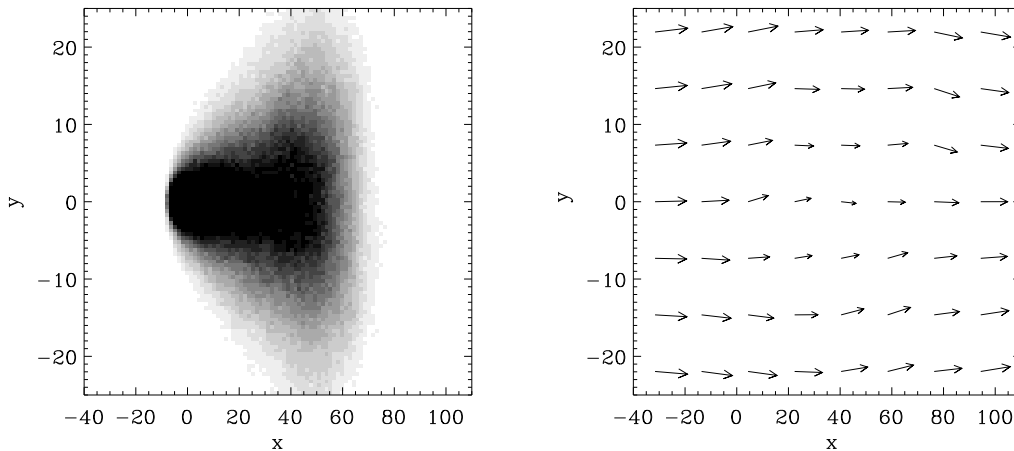


Figure 2: a) Segment density  $\rho(x, y, z = 0)$  and b) time-averaged perturbed flow field  $\mathbf{u}(x, y, z = 0)$  (right) for a chain with  $N = 200$  segments which is fixed at the origin with one end and subjected to a uniform flow in the  $x$ -direction with  $v = 0.02$ . Both EVI and HI are included and harmonic springs are used. The streamlines go around the region where the density of polymer segments is high, but the flow does not vanish there.

This partial draining is a superposition of two effects: The flow penetrates the polymer coil at any moment and due to thermal fluctuations the polymer also does not stay at a fixed location. The  $y$ -dependence of  $u_x$  shown in fig. 4 reveals a magnitude of the flow penetration of approximately one third of the unperturbed flow velocity. Furthermore there is a smaller decrease in the flow velocity which has a very long range, *i.e.* the unperturbed flow velocity is approached only very far away from the polymer coil.

The partial penetration of the deformed polymer coil also depends on the imposed flow velocity. Quantitative information about this velocity dependence is furnished by the overall drag force acting on the polymer, which may be measured in our simulation by the tension  $T_0$  in the first spring at the tether point. Even more revealing is the drag coefficient  $\Gamma = T_0/v$  for the whole coil. Its velocity dependence is plotted in fig. 4a). Without HI (upper curve) where the flow can freely penetrate the polymer coil – the so-called free draining case – each bead makes the same contribution  $\zeta$  to the coil drag coefficient independent of the flow velocity  $v$ , *i.e.*  $\Gamma = \zeta N$ . With HI (lower curve) there is only partial draining, *i.e.* the flow velocity inside the coil is reduced. Thus, the inner beads experience smaller drag forces and the total drag on the coil becomes smaller than in the free draining case. As the chain is stretched with increasing flow velocity, the flow penetration becomes stronger and finally the free draining value of  $\Gamma$  is approached.

This effect of the screening of the flow field due to HI and the related

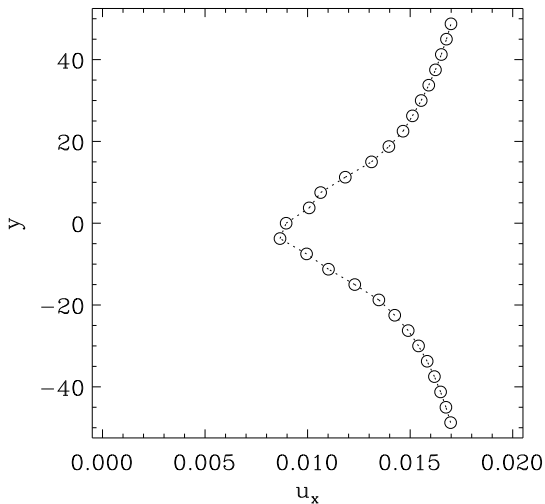


Figure 3: Spatially averaged  $x$ -component of the velocity field  $\mathbf{u}$  shown in fig. 2 as a function of  $y$ . The average was taken over the range  $0 \leq x \leq 40$  where the segment density is large. The smallest flow velocity is approximately one third of the unperturbed value  $v = 0.02$ .

reduction of the drag coefficient are also observed in the more didactic example of a two-bead system sketched in fig. 5a). The force required to keep the two beads fixed in a flow of velocity  $v$  is shown in fig. 5b) as a function of their distance  $d$ . The drag coefficient per bead  $\Gamma$  is seen to decrease with  $d$ . This mimics in a simple manner the situation for the polymer, where the average distance between the beads is smaller in the coiled than in the stretched state. The dependence of the drag coefficient on the shape of the polymer coil and therefore also on the flow velocity is in sharp contrast to the constant drag coefficient of a solid sphere given by Stokes law. In more complex systems such as polymer-coated colloidal particles similar deviations from Stokes' behavior can be caused also by a variety of other effects [44].

The elongation of the polymer is the result of a balance between the viscous drag exerted on the polymer by the flow and the thermal forces acting on the polymer. The stronger the screening of the flow field, the smaller is the drag force and also the elongation of the polymer. Hence, complementary to the overall drag coefficient is the polymer elongation which may be measured by the root mean square end-to-end distance  $R_E(v)$  shown in fig. 4b). Without HI (upper curve), where each bead experiences the same velocity-independent viscous drag, we find in the velocity range  $v = 0.001 - 0.01$  a behavior consistent with a power law  $R_E \propto v^\mu$  with  $\mu = 0.5$  and a transition to a linear dependence  $R_E \propto v$  for  $v > 0.1$ . Beyond this crossover, EVI become negligible because the polymer is uncoiled at large flow velocities. Including HI (lower curve) the onset of stretching is shifted to larger flow velocities. Around  $v = 0.5$  we find a maximal exponent of  $\mu = 1.5$  which is larger than without HI such that free draining behavior is approached for very large flow velocity. The shifted onset of chain stretching is another consequence of the screening of the flow inside the coil due to strong HI.

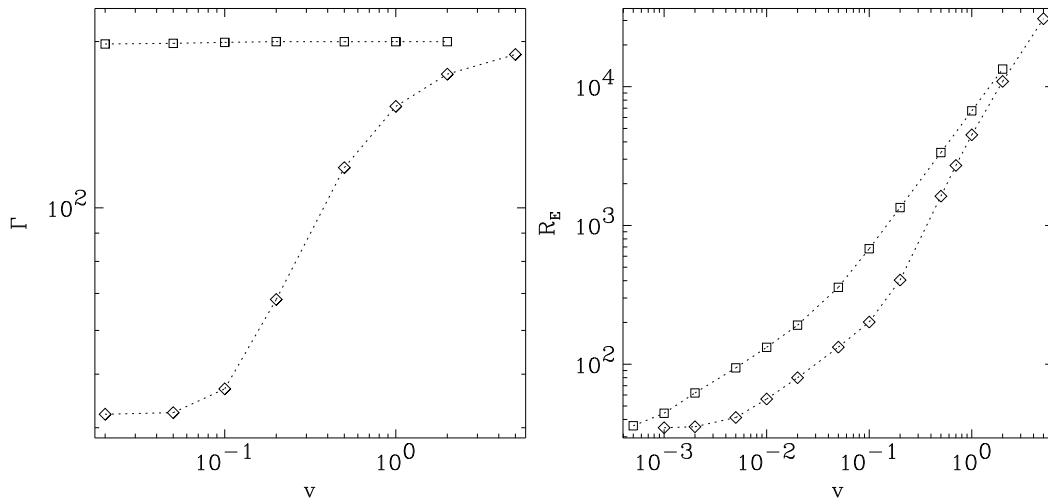


Figure 4: a) Total drag  $\Gamma$  experienced by the coil as a function of the imposed velocity  $v$  both with HI (diamonds) and without HI (squares). Otherwise the same model as in fig. 2 was used. b) Root mean square end-to-end distance  $R_E$  for the same two models.

With increasing flow velocity and polymer elongation the average distance between the beads increases and therefore the strength of the HI is reduced. This weakening is more pronounced close to the tethered end than near the free end as long as the chain is not fully stretched. At this stage of deformation the effects of HI vary significantly along the polymer chain. Finally for chains at very large  $v$  which are already strongly stretched the screening becomes negligible and the free draining behavior is approached.

$R_E(v)$  may be compared with analytical scalings for blob models, where the chain is described by a sequence of impenetrable [10] or free draining blobs [12]. For free draining chains with harmonic springs there is reasonable agreement with results for a blob model [12]. However, for impenetrable blobs  $R_E(v) \propto v^\mu$  with  $\mu = 2$  is predicted [10], which is considerably larger than the maximal exponent  $\mu \sim 1.5$  of the lower curve in fig. 4b). One reason for deviations between simulations and completely free or non-draining blob models is that when the polymer uncoils with increasing flow velocity, EVI and HI effects are continuously "switched off" such that the degree of penetration varies along the chain. This inhomogeneous process, which sets in at the tether point and with increasing flow velocity extends to the free chain end is not described by the blob models considered so far. As shown in Ref. [13, 14] it may be incorporated at least qualitatively in a generalized blob model where the blobs are composed of a non-draining inner core and a fully penetrable outer shell (f-shell).

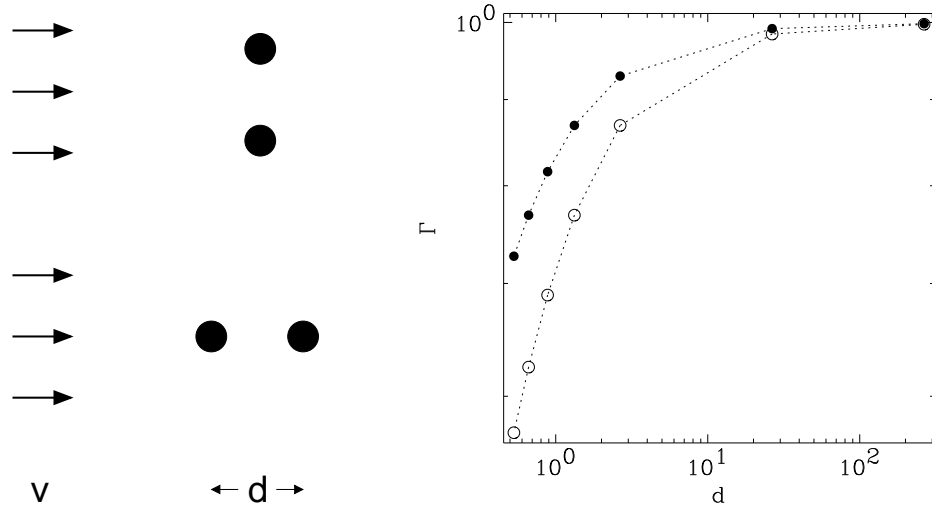


Figure 5: a) Two beads in a uniform flow are held at fixed positions where the relative position vector of length  $d$  is oriented either perpendicular (top) or parallel (bottom) to the flow. b) Drag coefficient  $\Gamma$  per bead as a function of the distance  $d$  for configurations with orientation perpendicular (solid circles) and parallel (open circles) to the flow. The flow velocity is  $v = 1.0$ , all other parameters have values as given in sect. 2.

The above considerations in principle carry over to the more realistic model with FENE springs. In that case, however, scaling regimes can be expected only for extremely long chains. An estimate shows that  $N \approx 10000$  is needed [12] which is not even reached in recent experiments [7, 18] where the number of Kuhn segments is less than 2000.

## 5 Conclusion

We have introduced a modified Brownian dynamics scheme, cf. eq.(12), by adding an artificial inertial term to the usual first order Langevin equation. This allows the integration time step to be chosen by a factor of 10 larger as for the usual case corresponding to vanishing mass, while maintaining a prescribed accuracy of the second moment of the equilibrium distribution for the positional degrees of freedom even for the steep potentials occurring in the models with finite extensibility or excluded volume interactions. In addition, we have implemented efficient algorithms for the treatment of excluded volume and hydrodynamic interactions that allow to overcome the chain length limitations of previous Brownian dynamics studies of polymers.

Formally the scheme eq. (12) is quite similar to that used in molecular dynamics simulations with a Langevin-thermostat, whereas its interpretation

is different [26, 45]. In molecular dynamics simulations the solvent is modeled explicitly as a collection of particles. Thus in that case noise and dissipation are a purely artificial means which is used to simulate a canonical ensemble while the masses of the particles represent true physical quantities. In our case in contrast, the masses of the particles are introduced as a computational device to speed up the simulation, while the stochastic and dissipative forces represent the solvent degrees of freedom which do not appear explicitly in the equations of motion.

In either case the length of the integration time which must be covered by the simulation is determined by the longest time scale of the problem which increases with the systemsize as  $N^2$ . The computational effort for the force calculations at each time step in our scheme is  $\sim \mathcal{O}(N^{2.25})$  (cf. sect. 3.1), *i.e.* the required CPU time increases as  $\sim \mathcal{O}(N^{4.25})$ . In comparison, for state of the art molecular dynamics simulations [43] which take full advantage of the short-range nature of the interaction potentials, the required CPU time increases only with the third power of the system size. However, in the case of molecular dynamics simulations the size of the system is the number of both solvent particles and polymer beads, which is beyond  $10^4$ . For Brownian dynamics simulations in contrast only the beads appear explicitly in the model and the system size is only of the order  $10^2$ . Comparing the chain lengths  $N \leq 60$  attained in recent nonequilibrium molecular dynamics simulations [46, 47] to our work, where  $N \leq 200$ , (500 if only EVI are considered) we find that saving the large overhead of solvent particles still outweighs the unfavorable scaling with the system size in current applications. Furthermore, the Brownian dynamics approach we choose allows easy inclusion or removal of various effects and arbitrary external flows. Both features may be difficult to realize in molecular dynamics simulations.

Simulation of the Brownian dynamics of bead–spring models for tethered polymers allows a detailed monitoring of various interactions between chain segments at different stages of the polymer deformation. Thus a test of the validity ranges of previous more coarse–grained model approaches becomes possible as described in more detail in Ref. [12]. Moreover, a thorough study of the polymer conformations and the flow field provides a starting point for the generalization and modification of these models such as the f-shell blob model for tethered polymers as introduced in Refs. [13, 14]. But not only static properties become amenable to investigation. The spectrum of relaxation times which characterizes the dynamics of conformational fluctuations about a stationary average conformation. The complete spectrum together with the associated modes can be extracted from simulation data as shown in Ref. [48]. This furnishes an important rheological function and gives further insight into the major motions that have to be accounted for in coarse–grained models.

When the flow undergoes a sudden change, there is no stationary average polymer conformation anymore. Instead, average quantities like the end-to-end distance become time-dependent. This time-dependent behavior is also investigated in Ref. [48] where single-mode models like the dumbbell have been challenged. In summary, the study of the behavior of tethered polymers in uniform flow is a first step in bridging the gap between the microscopic scale at which the interaction of single polymers and the flow takes place and the macroscopic continuum dynamics of polymer solutions.

In the context of biology, bead-spring type models similar to the one studied here, are used to model systems on very diverse levels of description ranging from individual protein molecules to entire tissues (see other contributions in this volume). Consequently, the techniques developed here may be of use in a much broader context than just polymer science. Furthermore hydrodynamic interactions are often important for the biological function of single macromolecules or more complicated aggregates. For example, a hydrodynamic steering effect has been found crucial for the reaction rates of protein-ligand binding [49]. Previously, the protein was considered as a rigid object while the methods described here allow to include the effects of its internal motions [50]. As a second interesting example we mention the computer study of a vesicle in Poiseuille flow using rather similar modelling approaches [51]. The vesicles were found to migrate towards the center of the flow which may be a relevant factor to inhibit mechanical degradation of red blood cells flowing through a blood-vessel. Finally, on a macroscopic level objects like vesicles or cells also behave much like viscoelastic fluids. Thus a basic question is again to determine the rheological functions from a more microscopic approach, a first step towards which was made here for polymer solutions.

## A Program tests

At thermal equilibrium the simulations can be compared with several well-known analytical results. The equilibrium distribution of the bond lengths can be calculated via the Boltzmann factor  $\exp(-\Phi/k_B T)$  using the spring potentials given in sect. 2. These analytically calculated distributions are compared in fig. 6 with the distributions obtained from simulations using these potentials for the springs.

For the Rouse model the bond length distribution is of course a Maxwellian. For the FENE model the distribution is sharply peaked around its maximum value so that it can be regarded as a good approximation to a freely jointed chain model. The bond length distribution for the Rouse model

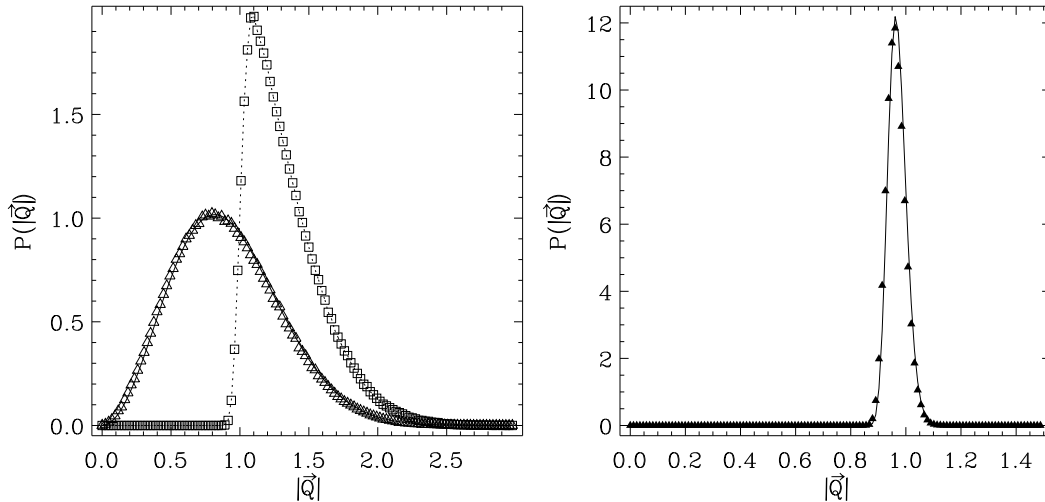


Figure 6: Probability distribution for the bond length  $|\mathbf{Q}| = |\mathbf{R}_{j+1} - \mathbf{R}_j|$  at thermal equilibrium for models with a) harmonic springs, both with (squares) and without (triangles) EVI, and b) FENE springs. In the latter case the addition of EVI has no effect on the bond length distribution since nearest-neighbor repulsion is included in the spring potential anyways. The solid lines are obtained by evaluating the Boltzmann factor  $\exp(-\Phi/k_B T)$  with the potentials given in sect. 2. The symbols give the results of the corresponding simulations for a chain with  $N = 100$  beads.

with excluded volume interactions reveals that the repulsive potential acts as a rather hard wall. Hence the distribution is deformed and its mean value is shifted to larger values. The addition of the excluded volume interactions to the FENE model of course leaves the bond length distribution unchanged because nearest neighbor repulsion is included anyway as described in sect. 2. As the analysis of the scaling of the end-to-end distance with the number of segments shows (see below), the effective bond length is rather close to the distance  $b = 0.961$  where the bond length distribution has its maximum.

A second more global test is the comparison of the numerically obtained end-to-end distance  $R_E$  as a function of the number of segments  $N$  with the scaling result due to Flory [1]

$$R_E = bN^\nu. \quad (18)$$

Here  $\nu$  is the scaling exponent while  $b$  gives an effective bond length. For any model with purely local interactions between the beads, it is well known that the exponent is  $\nu = 1/2$  [2]. In fig. 7a) we verify this behavior for the pure Rouse and FENE models. In these cases of course also the bond lengths are known so that we can contrast the numerical values with an analytical

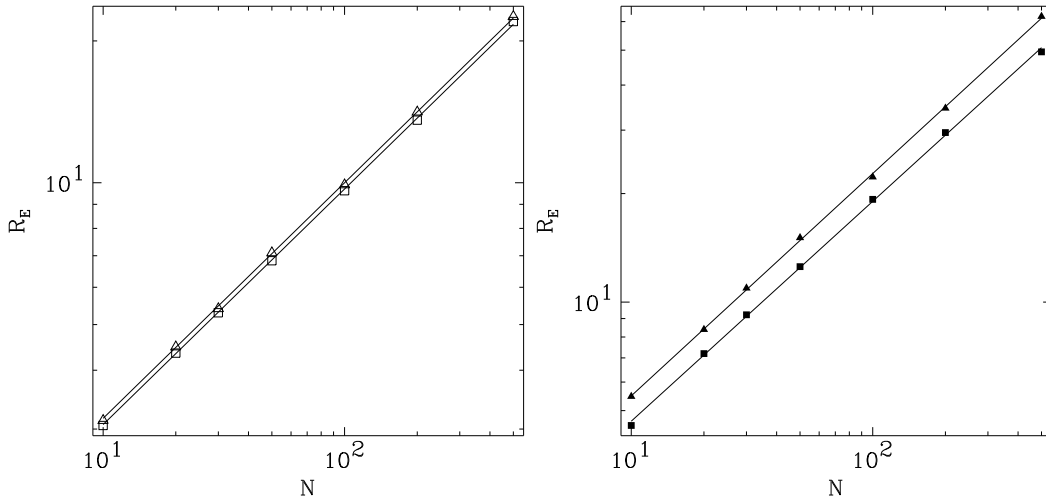


Figure 7: a) Equilibrium scaling of the end-to-end distance  $R_E$  with the number of segments  $N$  for the Rouse (open triangles) and FENE models (open squares). The solid lines are due to the scaling relation  $R_E = b\sqrt{N}$ , with the mean bond length  $b = 1.0$  for the Rouse chain and  $b = 0.961$  for the FENE chain. b) Equilibrium scaling of the end-to-end distance with the number of segments for the Rouse (solid triangles) and FENE models (solid squares) including the excluded volume effect. The solid lines are fits with a power law  $R_E = bN^\nu$ . The fit parameters are  $\nu = 0.617$ ,  $b = 1.33$  for the Rouse model and  $\nu = 0.610$ ,  $b = 1.15$  for the FENE model.

result without any adjustable parameters. The small difference between both models comes from the fact that the bond lengths for the Rouse ( $b = 1.0$ ) and FENE model ( $b = 0.961$ ) are slightly different. For both models there is a very good agreement with the numerical data even for rather short chains.

The excluded volume interactions change the scaling exponent for  $R_E$  from  $\nu = 1/2$  to  $\nu = 3/5$  neglecting a small correction to mean field theory [1]. In fig. 7b) we verify this behavior for the Rouse and FENE models with EVI. Since the prefactor is not known we fit a power law of the form of eq. (18) to the numerical data. The values of the exponents are  $\nu \sim 0.6$  for the models with either harmonic or FENE springs, which is in quite good agreement with the theoretical values. For the model with harmonic springs, the repulsive potential due to the excluded volume interaction leads to a considerable shift of the mean bond length to  $b = 1.33$ .

For the models with hydrodynamic interactions, a test is possible since all static properties at equilibrium are determined solely by the potential  $\Phi$  whereas the HI affect only the mobility. So one can simply compare the numerical values of the above quantities for the models with and without the

hydrodynamic effects. We find agreement within the statistical errors.

## References

- [1] P. J. Flory, *Statistical Mechanics of Chain Molecules* (Interscience Publishers, New York, 1969).
- [2] M. Doi and S. F. Edwards, *The Theory of Polymer Dynamics* (Clarendon Press, Oxford, 1986).
- [3] P.-G. deGennes, *Scaling Concepts in Polymer Physics* (Cornell University Press, Ithaca NY, 1981).
- [4] R. B. Bird, R. C. Armstrong, and O. Hassager, *Dynamics of Polymeric Liquids, Vols. I, II*, 2nd ed. (John Wiley, New York, 1987).
- [5] R. G. Larson, *Constitutive Equations for Polymer Melts and Solutions* (Butterworth, Stoneham MA, 1988).
- [6] T. T. Perkins, S. R. Quake, D. E. Smith, and S. Chu, *Science* **264**, 822 (1994).
- [7] T. T. Perkins, D. E. Smith, R. G. Larson, and S. Chu, *Science* **268**, 83 (1995).
- [8] S. Manneville *et al.*, *Europhys. Lett.* **36**, 413 (1996).
- [9] T. T. Perkins, D. E. Smith, and S. Chu, *Science* **276**, 2016 (1997).
- [10] F. Brochard-Wyart, *Europhys. Lett.* **23**, 105 (1993).
- [11] F. Brochard-Wyart, *Europhys. Lett.* **30**, 387 (1995).
- [12] R. Rzehak, W. Kromen, T. Kawakatsu, and W. Zimmermann, *Eur. Phys. J. E* **2**, 3 (2000).
- [13] R. Rzehak, D. Kienle, T. Kawakatsu, and W. Zimmermann, *Europhys. Lett.* **46**, 821 (1999).
- [14] D. Kienle and W. Zimmermann, F-shell Blob Model for a Tethered Polymer in Strong Flows, 2001, *Macromolecules* in print.
- [15] M. Murat and K. Kremer, *J. Chem. Phys.* **108**, 4340 (1998).
- [16] H. C. Öttinger, *J. Chem. Phys.* **86**, 3731 (1987).

- [17] J. J. Magda, R. G. Larson, and M. E. Mackay, *J. Chem. Phys.* **89**, 2504 (1988).
- [18] R. G. Larson, T. T. Perkins, D. E. Smith, and S. Chu, *Phys. Rev. E* **55**, 1794 (1997).
- [19] M. Fixman, *Macromolecules* **19**, 1204 (1986).
- [20] F. Brochard-Wyart, H. Hervet, and P. Pincus, *Europhys. Lett.* **26**, 511 (1994).
- [21] Y. Marciano and F. Brochard-Wyart, *Macromolecules* **28**, 985 (1985).
- [22] R. B. Bird and H. C. Öttinger, *Annu. Rev. Phys. Chem.* **43**, 371 (1992).
- [23] J. D. Schieber and H. C. Öttinger, *J. Chem. Phys.* **89**, 6972 (1988).
- [24] P. E. Rouse, Jr., *J. Chem. Phys.* **21**, 1272 (1953).
- [25] H. R. Warner, Jr., *Ind. Eng. Chem. Fundam.* **11**, 379 (1972).
- [26] K. Kremer and G. S. Grest, *J. Chem. Phys.* **92**, 5057 (1990).
- [27] R. Zwanzig, *Adv. Chem. Phys.* **15**, 325 (1969).
- [28] W. Zylka and H. C. Öttinger, *J. Chem. Phys.* **90**, 474 (1989).
- [29] H. C. Öttinger and Y. Rabin, *J. Rheol.* **33**, 725 (1989).
- [30] H. C. Öttinger, *Stochastic Processes in Polymeric Fluids* (Springer, Heidelberg, 1996).
- [31] B. H. Zimm, *J. Chem. Phys.* **24**, 269 (1956).
- [32] D. L. Ermak and J. A. McCammon, *J. Chem. Phys.* **69**, 1352 (1978).
- [33] P. E. Kloeden and E. Platen, *Numerical Solution of Stochastic Differential Equations* (Springer, Heidelberg, 1992).
- [34] J. Hendriks, T. Kawakatsu, K. Kawasaki, and W. Zimmermann, On Semiflexible Polymers in an Anisotropic Medium: A Phenomenological Model, unpublished.
- [35] G. H. Golub and C. F. v. Loan, *Matrix Computations*, 2nd ed. (John Hopkins University Press, Baltimore MD, 1989).
- [36] M. Fixman, *Macromolecules* **19**, 1195 (1986).

- [37] A. Björck and G. Dahlquist, *Numerische Methoden*, 2nd ed. (R. Oldenbourg, München, 1979).
- [38] W. H. Press *et al.*, *Numerical Recipes in C*, 2nd ed. (Cambridge University Press, Cambridge UK, 1990).
- [39] M. P. Allen and D. J. Tildesley, *Computer Simulation of Liquids* (Clarendon Press, Oxford, 1987).
- [40] D. C. Rapaport, *The Art of Molecular Dynamics Simulation* (Cambridge University Press, Cambridge UK, 1995).
- [41] D. Frenkel and B. Smit, *Understanding Molecular Simulation*, 3rd ed. (Academic Press, New York, 1998).
- [42] D. C. Rapaport, in *Microscopic Simulations of Complex Flows*, edited by M. Mareschal (Plenum Press, New York, 1990), p. 57.
- [43] G. S. Grest, B. Dünweg, and K. Kremer, *Comp. Phys. Commun.* **55**, 269 (1989).
- [44] D. Kienle, R. Rzehak, W. Zimmermann, in preparation.
- [45] T. Schneider and E. Stoll, *Phys. Rev. B* **17**, 1302 (1978).
- [46] C. Pierloni and J. P. Ryckaert, *Macromolecules* **28**, 5097 (1995).
- [47] C. Aust, M. Kröger, and S. Hess, *Macromolecules* **32**, 5660 (1999).
- [48] R. Rzehak and W. Zimmermann, Dynamics of Strongly Deformed Polymers in Solution , 2001, submitted to *Phys. Rev. Lett.*.
- [49] D. Brune and S. Kim, *Proc. Natl. Acad. Sci. USA* **91**, 2930 (1994).
- [50] in *Proteins: A Theoretical Perspective of Dynamics, Structure and Thermodynamics*, Vol. 71 of *Adv. Chem. Phys.*, edited by C. L. Brooks, M. Karplus, and B. M. Pettitt (John Wiley, New York, 1988).
- [51] G. Ristow, I. Cantat, W. Zimmermann, and C. Misbah, in preparation.